

# Doppler imaging of stellar surface structure

## VI. HD 129333 = EK Draconis: a stellar analog of the active young Sun

K.G. Strassmeier<sup>1,\*</sup> and J.B. Rice<sup>2,\*</sup>

<sup>1</sup> Institut für Astronomie, Universität Wien, Türkenschanzstraße 17, A-1180 Wien, Austria (strassmeier@astro.ast.univie.ac.at)

<sup>2</sup> Department of Physics, Brandon University, Brandon, Manitoba R7A 6A9, Canada (rice@BrandonU.ca)

Received 3 September 1997 / Accepted 29 September 1997

**Abstract.** We present the first Doppler images of the single G1.5V-star EK Draconis from high-resolution CFHT spectra obtained in 1995. EK Dra is an important target for investigating the evolution of stellar magnetism because it resembles the rapidly-rotating young Sun. From the inversion of a total of 12 spectral lines we reconstruct several cool spots at low and medium latitudes but the dominating feature is located consistently at a latitude of  $\approx 70\text{--}80^\circ$ , thus, at far higher latitudes than where our Sun shows spots. In fact, our data indicate that this feature could be an appendage of a larger polar cap-like spot as seen on other rapidly-rotating stars, however, due to the small  $v \sin i$  of just  $17.3 \pm 0.4 \text{ km s}^{-1}$  the cap's existence remains inconclusive. Spot temperatures between  $\Delta T \approx 1200 \text{ K}$  and  $400 \text{ K}$  are recovered. We have used the non-parametrized convective-flux description of Canuto & Mazzitelli for our input model atmospheres and found good agreement with local line profiles computed from standard mixing-length atmospheres.

New phase-resolved *UBVRI* data spanning the 1996/97 observing season indicate a surprisingly short photometric period of  $2.599 \pm 0.001$  days, which is different by 7% from the longest seasonal period found so far but in good agreement with the long-term photometric period of 2.605 days. We interpret these differences as being due to differential surface rotation and adopt the long-term photometric period to be the rotation period of EK Dra. Our data also confirms the continuing decline of the mean brightness seen since 1994 and we suspect the high-latitude feature to be the cause.

**Key words:** stars: activity of – stars: imaging – stars: individual: EK Dra – stars: late-type – starspots endtrivlist

### 1. Introduction

Doppler imaging is a technique that uses the relation between the radial velocity and the intensity of a point on a rotating stellar

surface and its projected signature in the broadened line profile to recover the stellar surface temperature distribution (Deutsch 1958, Vogt et al. 1987, Rice 1989 a.o.). Cool spots on the surface of late-type stars produce distortions in the line profiles that can be modelled throughout a rotational cycle. Modern approaches invert the observations to recover a unique surface temperature distribution within an otherwise ill-posed problem. It is this spot distribution that we believe must be a signature of the magnetic surface field and eventually the underlying stellar dynamo. The aim of this series of papers is to systematically obtain Doppler images of active stars from various parts in the Hertzsprung-Russell diagram.

The discovery of polar starspots on the RS CVn binary HR 1099 by Vogt & Penrod (1983) – at a region where the Sun has no spots at all – fostered intensive investigations of spotted stars of all evolutionary stages but focused mostly on rapidly-rotating giants and subgiants in close binary systems. Bright and rapidly rotating dwarf stars are relatively rare and are mostly spun-up components in close binary systems. Only three of them have published Doppler images: ER Vulpeculae, G0V+G5V (Piskunov 1996), YY Geminorum, M1Ve+M1Ve (Hatzes 1995), and V471 Tauri, K2V+wd (Ramseyer et al. 1995). But with the advent of ever better CCDs and spectrographs, and 10m-class telescopes, altogether four, *single*, main-sequence stars have been Doppler imaged to date: the Pleiades-age K2-star LQ Hydrae (Strassmeier et al. 1993, Saar et al. 1994, Rice & Strassmeier 1997), the even younger K0 ZAMS star AB Doradus (Kürster et al. 1994, Collier-Cameron & Unruh 1995, Collier-Cameron 1995, Unruh et al. 1995, Hussain et al. 1997, Donati & Collier-Cameron 1997), and the two low-mass Pleiades stars HII 686 (K5V) and HII 3163 (M0V) by Stout-Batalha & Vogt (1996). Polar spots or, say, very high-latitude spots were found on all of them. However, these stars are of significantly different age, mass, temperature, or radius than the Sun and one could argue that they are poor comparisons for the present-day active Sun.

In this paper we present the first Doppler image of a single, solar-like star that is rotating rapidly enough to allow the application of the Doppler-imaging technique and has the Sun's

\* Visiting Astronomer, Canada-France-Hawaii Telescope, operated by the National Research Council of Canada, the Centre National de la Recherche Scientifique de France, and the University of Hawaii

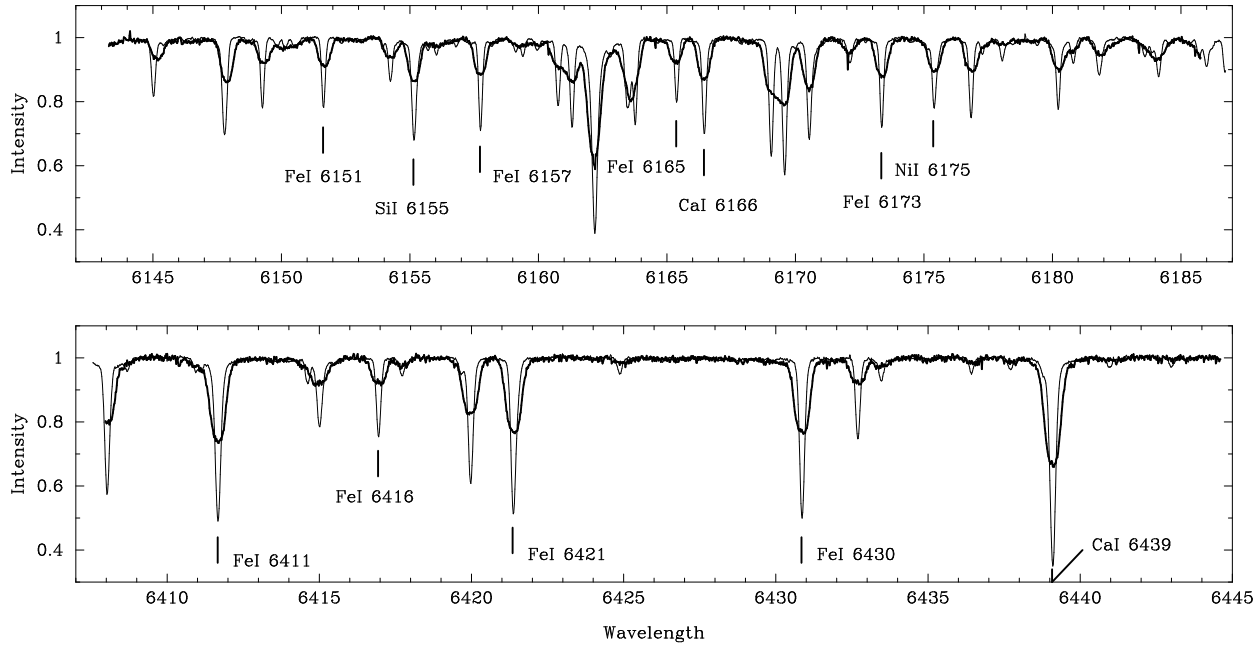


**Fig. 1.** Two examples of the spectra used in the Doppler-imaging analysis in this paper. In both panels the thick line is a spectrum of EK Draconis and the thin line a spectrum of the G0V M-K standard star  $\beta$  Comae. Resolving power is 120,000, S/N for EK Dra is estimated to be around 250:1. The spectral lines for Doppler imaging are marked.

spectral type of G2V with a rotation period of around 2.7 days. The star is EK Draconis = HD 129333, having an ultraviolet spectrum rich with strong and variable chromospheric emission lines (Dorren & Guinan 1994), frequent low-level flaring of the transition-region lines CIV and SiIV (Saar & Bookbinder 1997), the highest known Ca II H and K emission level of any single, early G-type star (Soderblom 1985), strong non-thermal radio emission (Güdel et al. 1995a), and rotationally modulated X-ray emission (Güdel et al. 1995b) from a 7–18 MK hot corona with a x-ray luminosity of  $\log L_X \approx 29.8 \text{ erg s}^{-1}$  (Güdel et al. 1997a, 1997b). Its *Hipparcos* space motions confirm that the star is a member of the Pleiades moving group which places its age to close to 70 Myr. Table 1 is a summary of relevant astrophysical parameters.

EK Draconis is also photospherically active. Its light variability was discovered independently by Dorren & Guinan (1994) in 1983 and later by Chugainov et al. (1991) in 1991. Radick (1991) described the annual Lowell Observatory Strömgren data from as early on as 1983 and throughout 1989. Phase-resolved photometric monitoring from 1994 to 1996 was recently presented by Strassmeier et al. (1997a) and included data obtained by Guinan and collaborators. Since 1994 the broad-band *V* amplitude varied between 0.05–0.15 mag on a time scale of a few months, indicating some short-term restructuring of spots on the stellar surface, and also revealing a distinctive, monotonic decrease of the average brightness by 0.05 mag. Earlier, Dorren & Guinan (1994) and Dorren et al. (1995) had plotted the mean differential *V*-brightness from 1983 through 1994 and suggested a cyclic variability with a period of

12–14 years<sup>1</sup>. The simultaneously observed Mt. Wilson Ca II H and K emission index was found to increase during that time, suggesting that the star became fainter as its mean level of chromospheric activity rose.

## 2. Observations

All spectroscopic observations in this paper were obtained with the *f/4 Gecko* coude spectrograph at the 3.6-m Canada-France-Hawaii telescope (CFHT) in March 12–17, 1995. Together with the 2k-Lick CCD the dispersion of 1.6 Å/mm provided a resolving power of 120,000 ( $2.5 \text{ km s}^{-1}$ ) in a useful wavelength range of around 50 Å. Seeing was always better than 1'' and all integrations were set at an exposure time of  $5 \times 10 \text{ min}$  and have typical signal-to-noise ratios of 250:1 and were centered alternately at 6420 Å and 6160 Å. This sequence allowed a sampling of better than 0.1 phases with a total of 14 spectra in the 6160-Å region and 14 spectra in the 6420-Å region. Fig. 1 displays representative spectra for each of the two wavelength regions. No water-vapor lines above the nominal noise level are obvious in these spectra. The reduction procedure was identical to that in our first paper on LQ Hydrae (Strassmeier et al. 1993) obtained with the *f/8* camera and we refer the reader to that paper.

Contemporaneous and simultaneous photometric observations were kindly provided by Dr. E. F. Guinan and were already included in the analysis in Strassmeier et al. (1997a).

<sup>1</sup> We note that the last data point in the long-term lightcurve in Fig. 8 of Dorren & Guinan (1994) – that was trendsetting for the cyclic variability – appears shifted by +0.02 mag in the same diagram in Dorren et al. (1995).

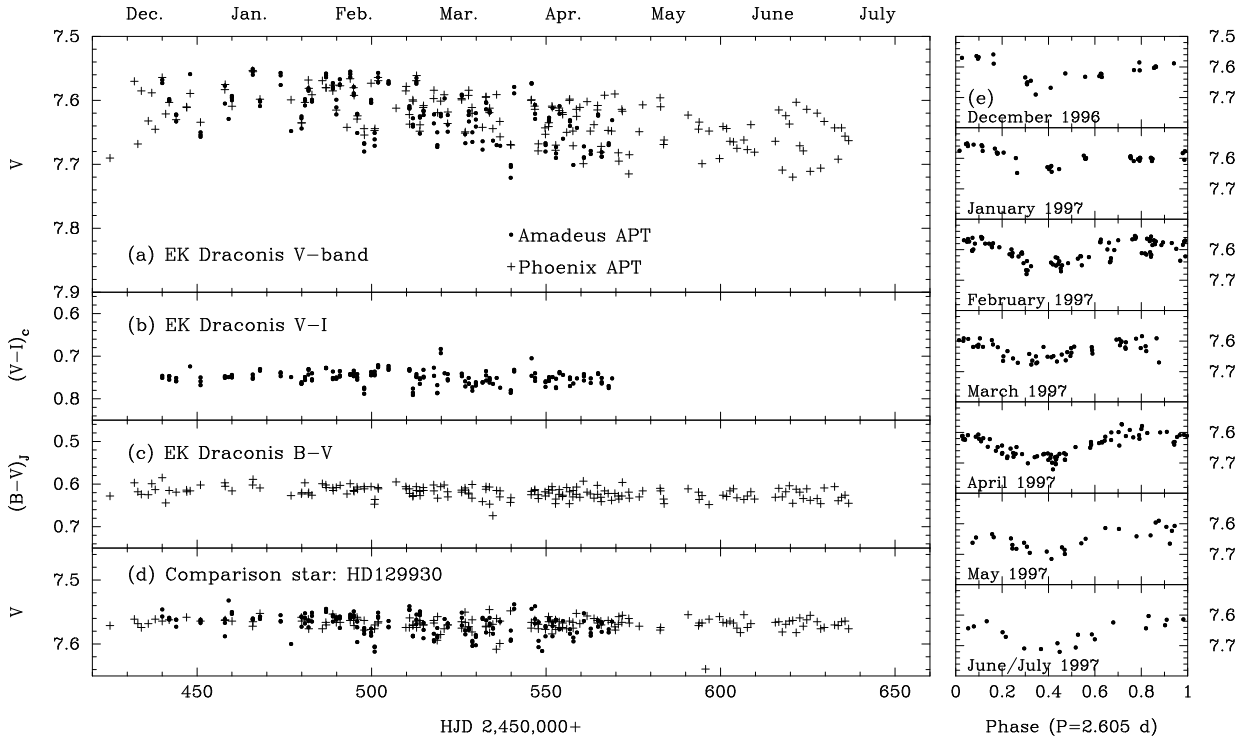


**Fig. 2a–d.** Plots showing the results from photometric monitoring of EK Draconis throughout 1996/97. Since early March, the overall  $V$  brightness decreased by approximately 0.07 mag within four months (panel a), while the  $V - I_C$  and  $B - V$  colors remained constant (panels b and c, respectively). Panel d plots the  $V$  magnitudes of the comparison star from our all-sky solution. The seven vertical panels (labeled e) are the monthly, phased light curves from December 1996 through June/July 1997 and show essentially identical light-curve shape and amplitude. This, and the overall dimming at constant colors, implies a relatively stable, surface-integrated temperature over time and suggests an increase in spottedness at higher latitudes.

In 1996 and 1997, further photometry has been obtained with the Wolfgang-Amadeus 0.75m Vienna Observatory Twin Automatic Photoelectric Telescope (WA-APT, Strassmeier et al. 1997b) and the 0.25m Phoenix-10 APT. Both telescopes are located at Fairborn Observatory in Washington Camp in southern Arizona. Altogether, 171 new  $UBV$  measures and 168  $VRI$  measures were obtained, each the mean of three readings between the variable and the comparison star. The WA-APT data were transformed to the Cousins  $V(RI)_C$  system and used HD 129930 and HD 129798 as the comparison and check stars respectively while the Phoenix-10 APT data were obtained with Johnson  $UBV$  filters and had the same comparison and check stars. An all-sky solution from about sixty standard stars observed with the WA-APT throughout the entire 1996/97 season gives the following magnitudes for the comparison and check star. HD 129930:  $V=7.567$  mag,  $R_C=7.317$  mag,  $I_C=7.067$  mag, and for HD 129798:  $V=6.236$  mag,  $R_C=5.986$  mag, and  $I_C=5.742$  mag (errors are typically 0.01 mag). The standard error of a nightly mean from the overall seasonal mean is for the WA-APT 0.004 mag in  $V$  and 0.006 mag in  $R_C$  and  $I_C$ , and for the Phoenix-10 APT 0.009 mag in  $B$  and  $V$ , and 0.013 mag in  $U$ .

**Table 1.** Astrophysical data of EK Draconis

Parameter	Value
Spectral type	G1.5V
$V_{\max}$	7.51 in 1994.2
$V_{\min}$	7.72 in 1997.5
Distance (Hipparcos)	33.9 pc
$\log g$	4.5
$T_{\text{eff}}$	$5870 \pm 50$ K
$(B - V)_{\text{Hipparcos}}$	$0.626 \pm 0.018$ mag
$v \sin i$	$17.3 \pm 0.4$ km s $^{-1}$
Inclination $i$	$60^\circ$
Rotation period	$2.6050 \pm 0.0003$ days
Micro turbulence $\xi$	$2.0$ km s $^{-1}$
Macro turbulence $\zeta_R = \zeta_T$	$4.0$ km s $^{-1}$
Chemical abundances	solar

### 3. Photometric monitoring

#### 3.1. The light-curve variability

Fig. 2 is a plot of our new APT observations of EK Draconis from December 1996 through July 1997. The full amplitude of the  $V$ -light curve remained around 0.10 mag but is subject to small but nevertheless significant changes after one

month. The smallest amplitudes were seen in January and March ( $0.075 \pm 0.005$  mag) and the largest in April with  $0.105 \pm 0.005$  mag. Actually, the “scatter” in our monthly  $V$ -light curves in Fig. 2 may indicate subtle changes on even shorter time scales. The location of the light-curve minimum remained stable at  $0.3\text{--}0.4$  within the  $\approx 200$  continuous nights of observations (approx. 80 stellar rotations). However, from early March on, a steady dimming of the maximum and minimum brightness became obvious and continued up to the end of our time series in mid July 1997. Such a dimming, along with an almost constant light-curve amplitude, is not an untypical behaviour of spotted stars but contrary to observations of some more active, heavily spotted RS CVn-type binaries (e.g. Strassmeier et al. 1997a, Henry et al. 1995). It can not be explained with a simple simultaneous growth of *all* spots because that would increase the amplitude when the star becomes fainter unless the spots are all circumpolar or at least at high latitude. In some of the most spotted RS CVn’s it can even lead to a smaller amplitude because the asymmetry of the spot distribution becomes smaller the larger the spots grow. An increasing dimming with a constant amplitude must – in a weakly to moderately spotted star like EK Draconis – have a more global reason, e.g. due to the migration of spots from the equatorial regions to circumpolar regions (the other way around would cause a brightening as was shown by the simulations in Strassmeier & Bopp 1992), or a growing polar spot competing with a decreasing plage component. Since the  $V - I_C$  and  $B - V$  color curve remained constant throughout the observing season we may – tentatively – also exclude global temperature effects, i.e. due to a cooling of all spots, or a general temperature decrease of the surrounding unspotted photosphere.

Because no dimming is obvious in the preceding three months in Dec. 1996 through Feb. 1997, and the (formally) largest amplitude was seen shortly after the decrease began, and the light-curve minimum remained fixed at phase  $0.3\text{--}0.4$ , we believe that the cause of the extra dimming is an increase of the spottedness at high latitudes.

### 3.2. The rotational period

Since EK Draconis is a single star we have no reference period – like the orbital period in binaries – and thus completely rely on the detected photometric variations to determine the average rotation period of the star. However, a surface spot distribution with two spot groups separated by  $\approx 180^\circ$  in longitude could mimic a photometric period that is only one half of the true rotation period. To exclude such a possibility we first examined the long-term  $V$ -light curve morphology and searched for eventual phase jumps within a few photometric cycles, but none occurred within our observations. Moreover, we see a rather asymmetric light curve shape when phasing the data with the best photometric period (e.g. in December 1996 and January 1997 in Fig. 2) indicating a slightly double-peaked light curve. Therefore we feel safe in adopting the photometric period to be the average rotation period of EK Draconis.

Strassmeier et al. (1997a) performed a period analysis of the then available photometric data up to early 1996 and found a long-term average photometric period of  $2.6050 \pm 0.0003$  days from the combination of 3 years of  $V$  and  $y$ -band data. Different seasonal periods between 1994 and 1996 indicated that changes of the spot distribution are likely to occur, possibly due to differential rotation. The best photometric period during our spectroscopic observations for Doppler imaging in 1994/95 was  $2.602 \pm 0.001$  days, while in 1995/96 it was  $2.603 \pm 0.003$  days, and in 1993/94 even  $2.796 \pm 0.026$  days. Dorren & Guinan (1994) had found a period of  $2.70 \pm 0.02$  days from their early photometry in 1983 and estimated 2.74 days for their photometry from 1988. The latter value was also used by Scheible & Guinan (1994) to model their APT data from 1990–1994 although no specific period determination (e.g. with error bars) was given in that paper. Our new  $V$ -band data from 1996/97, as discussed in the previous section and plotted in Fig. 2, indicate a surprisingly short but precise period of  $2.5992 \pm 0.0010$  days from a minimization of the squared residuals of a Fourier fit using the program of Breger (1990). Because sampling is reasonably good – up to four light-curve points during *every* clear night throughout the whole observing season – the small error of just 0.25% indicates a stable spot pattern in longitude suggestive of almost rigid rotation if interpreted within the usual framework of differential surface rotation.

The spectroscopic data in this paper were phased with the average long-term photometric period between 1994 through 1997, probably being the best approximation to the true rotation period, while the zero point is just an arbitrary time adopted from Strassmeier et al. (1997a) to be consistent with their light-curve phases:

$$2,449,403.0 + 2.60498 \pm 0.00030 \times E . \quad (1)$$

We note that the choice of the period for phasing our spectra of EK Draconis is not as critical as it usually is for short-period stars because all spectroscopic data were gathered within less than two consecutive rotational cycles and even an error of 0.1% would lead only to a relative phase uncertainty of 0.001 (as a comparison, rotational phase smearing during the 50-min integration time amounts to 0.013).

## 4. Multiline Doppler imaging

### 4.1. The inversion code *TEMPMAP*

Our Doppler-imaging code has been extensively described and tested by Rice et al. (1989) and reviewed by Piskunov & Rice (1994) as well as in previous papers of this series and we refer the reader to these papers. For the 1995 CFHT data of LQ Hydrae we first applied a significantly modified version which included additional input from absolute instead of relative photometry to further constrain the solution (Rice & Strassmeier 1997). However, for EK Draconis we have only single-band Strömgren  $y$  photometry that is contemporaneous to the spectroscopic observations and for the analysis in this paper we turned off the absolute-photometry option in *TEMPMAP*. Consequently, all

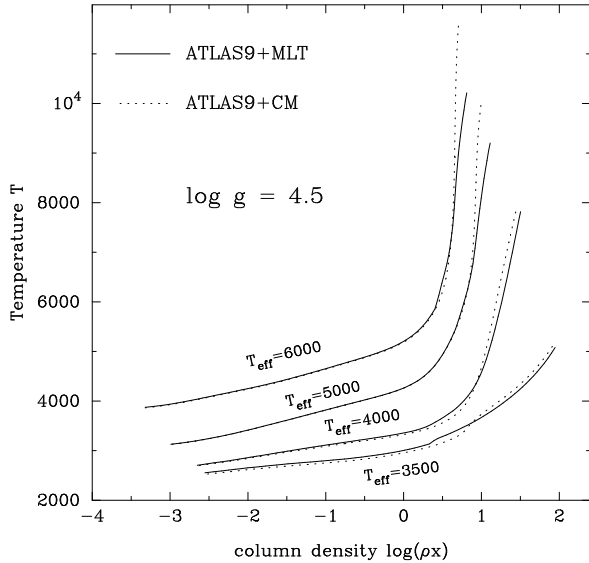


**Fig. 3.** A comparison of the ATLAS-9 model atmospheres computed with the mixing-length theory (MLT) and the Canuto & Mazzitelli (CM) convection model. At the expected temperatures of EK Dra the differences between the two models are only obvious at the very deep layers of the photosphere.

**Table 2.** Atomic data of the main spectral lines used for Doppler imaging

Element	Wavelength (Å)	$\log gf$ (-)	$\chi$ (eV)	# of blends	$W_\lambda$ (mÅ)
Fe I	6151.617	-3.80	2.176	3	49
Si I	6155.134	-0.63	5.619	3	82
Fe I	6157.725	-1.46	4.076	4	64
Fe I	6165.361	-1.75	4.143	1	41
Ca I	6166.440	-1.20	2.521	1	65
Fe I	6173.341	-3.20	2.223	1	69
Ni I	6175.360	-0.56	4.089	4	56
Fe I	6411.647	-0.82	3.654	7	182
Fe I	6416.929	-1.02	4.794	2	61
Fe I	6421.349	-2.20	2.279	6	169
Fe I	6430.844	-2.10	2.176	10	172
Ca I	6439.075	+0.47	2.526	9	264

synthesized photometry of EK Draconis has an arbitrary zero point and it is thus only the light-curve *shape* that contributes to the Doppler-imaging solution. Besides that, our approach includes a full spectrum synthesis for the local line profile(s) from a solution of the equation of transfer at each of the 2592 surface pixels in each of the 12 wavelength regions and simultaneous inversion of up to twenty lines using either a maximum-entropy or a Tikhonov regularisation. All computations were performed on a DEC AXP 250-4/266 workstation and required on average 30 CPU-minutes for one run with 10 blends and 15 iterations.

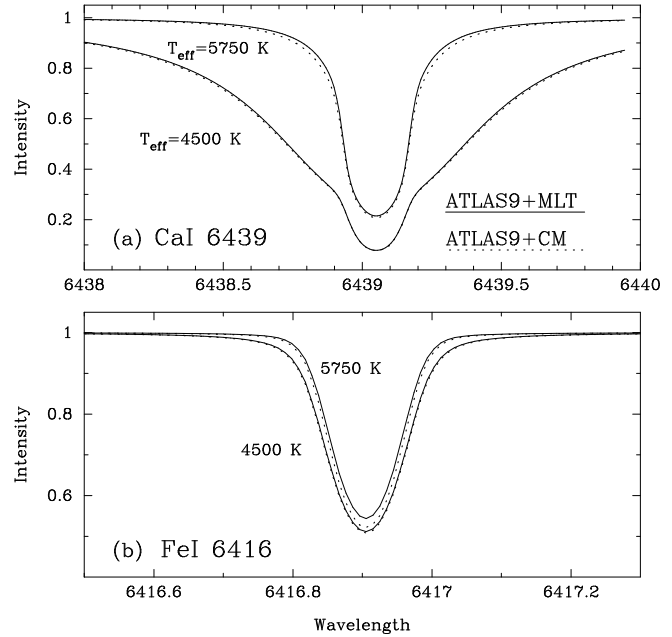


**Fig. 4a and b.** Two plots showing local line profiles for the strong Ca I-6439 line (a) and the weak Fe I-6416 line (b). Each panel compares the profiles from two ATLAS-9 model atmospheres, each computed with the mixing-length theory (MLT; continuous profiles) and the Canuto & Mazzitelli (CM; dotted profiles) convection model.

#### 4.2. The input model atmospheres

A grid of ten model atmospheres, each with 72 layers, and temperatures between  $T_{\text{eff}} = 4000$  and 6250 K and fixed  $\log g = 4.5$ , were taken from the CD-ROM distributed by Kurucz (1993) and are supplied in a pre-tabulated form. For temperatures not within  $\pm 10$  K of one of the tabulated input atmospheres we interpolate between them. For each surface temperature, local line profiles are computed for all spectral features within the main wavelength regions listed in Table 2. This is done under the assumption of LTE, solar abundances, a microturbulence of  $2.0 \text{ km s}^{-1}$ , and a macroturbulence of  $4.0 \text{ km s}^{-1}$ . The disk integrated equivalent widths in Table 2 ( $W_\lambda$ ) were measured off a phase-averaged spectrum by fitting a single Gaussian and are intended for comparison purposes only. Note that equivalent width is an implicit free parameter in our code and is determined by the various model atmospheres, the adopted chemical abundances, and the line transition probabilities.

Due to the very small rotational broadening of the spectral lines of EK Dra ( $v \sin i = 17.3 \text{ km s}^{-1}$ ) – and thus the greatly increased importance of the local line profile computation – we first compared the standard Kurucz (1993)-atmospheres with a set of model atmospheres that were computed with the Canuto & Mazzitelli (1992) (CM) convection model (kindly provided by F. Kupka, see Kupka 1996). This replaces the parametrized mixing-length theory (MLT) as implemented in ATLAS-9 and discussed, e.g. in Castelli et al. (1997). The main difference between these two sets of atmospheres is that in the CM model the onset of efficient convection already appears at temperatures

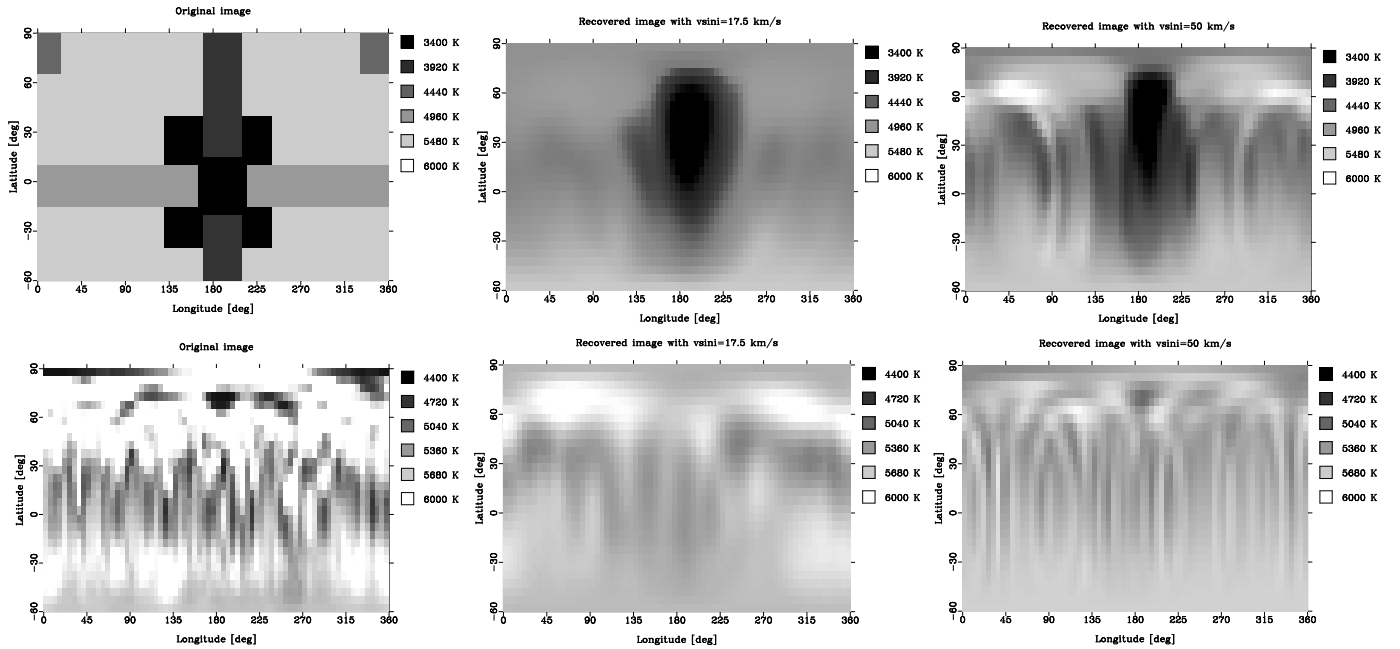


**Fig. 5.** Two test patterns and their recovered images with two different rotational velocities. The left column are the artificial input images, the middle column the reconstructions with  $v \sin i = 17.5 \text{ km s}^{-1}$ , and the right column with  $v \sin i = 50 \text{ km s}^{-1}$ . Line and stellar parameters were identical to the ones found for EK Dra.

approximately 1000 K cooler than in the mixing-length theory and results in a divergence of the atmospheres' temperature gradient at high optical depths. Although not as obvious at solar-type effective temperatures as for A–F, and again M-type dwarf stars the computed equivalent width of lines formed in the deep photosphere can change by a few percent. Within this context it is somewhat surprising though that the synthesized  $b - y$  color for the Sun is better matched by the MLT (with or without overshoot) than by the CM model (Castelli et al. 1997, Smalley & Kupka 1997). However, as mentioned by these authors, the uncertainties of the solar  $b - y$  color precludes any conclusive statement.

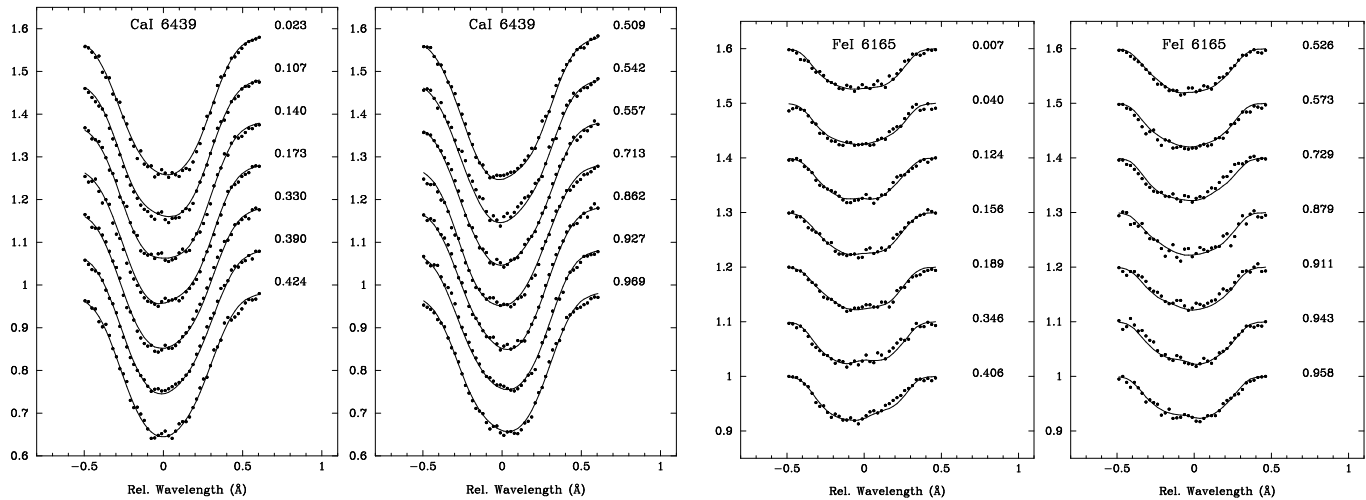
Fig. 3 compares the two model atmospheres for effective temperatures of 3500, 4000, 5000, and 6000 K. Although the differences between MLT and CM can be large at very high column densities, i.e. for regions in the convection zone rather than in the photosphere, they do not propagate significantly into the line-forming regime of our spectral lines for Doppler imaging. For example, the models for an effective temperature of  $\approx 5000 \text{ K}$  agree especially well below a logarithmic column density of  $\log(\rho x) \approx 0.0$ , i.e.  $\tau_{\text{Ross}} \approx 0.1$ , where almost no difference between CM and MLT is obvious in Fig. 3 and, consequently, we expect only weak, if any, influence on the spot's local line profiles because the effective photospheric temperature of EK Dra is near 5850 K and the spotted regions usually 800–1000 K cooler.

Fig. 4 shows the local line profiles of two of our Doppler-imaging lines: the “strong”, almost saturated, CaI-6439 line and the weak FeI-6416 line. These computations are made with the same subroutine that is employed in TEMP MAP. Compared in

these figures are profiles from the two sets of atmospheres for effective temperatures of 5750 K and 4500 K. The two temperatures may represent the local temperature of the unspotted photosphere of EK Dra and of its coolest spots. The differences at the expected umbral spot temperature of around 4500–5000 K are very small – always less than 0.005 in residual intensity or 0.1% in equivalent width, i.e., barely noticeable in the profiles in Fig. 4 – while at the photospheric temperature of close to 5750 K the differences become more obvious, but still reach at most only 0.02 in intensity in the core of the weak FeI-6416 line and 0.03 in the wings of the strong CaI-6439 line. The differences in equivalent width are accordingly  $\approx 1\%$  for CaI 6439 Å and  $\approx 4\%$  for FeI 6416 Å in the sense that the CM profiles always have the larger equivalent widths. The differences of the continua between CM and MLT atmospheres amounts to 2% at 5750 K, and to 0.3% at 4500 K. However, notice that in Fig. 4 both, spotted and unspotted, profiles are scaled to the same relative continuum but that the spot continuum is usually only  $\approx 10\%$  of the photospheric continuum and the larger differences in the weak line become smaller by roughly a factor of ten. When using the CM atmospheres instead of the standard MLT atmospheres for the line-profile inversion, we found no noteworthy difference in the resulting Doppler maps and conclude that our maps of EK Dra do not suffer from an inadequate description of the convective flux in a late-type stellar atmospheres.

#### 4.3. Numerical simulations with $v \sin i = 17.5 \text{ km s}^{-1}$

At the resolving power of  $\lambda/\Delta\lambda=120,000$  (i.e.  $2.5 \text{ km s}^{-1}$  or  $0.05 \text{ \AA}$ ) and a full width of the lines at continuum level of  $2(\lambda/c)v \sin i = 0.77 \text{ \AA}$  we have 15 resolution elements across



**Fig. 6.** Observed and computed line profiles for two representative spectral lines of EK Draconis. Left, the Ca I 6439 line and, right, the Fe I 6165 line with a smaller equivalent width by about a factor of six. The dots are the observations and the lines are the fits. Rotational phase is indicated on the right side of each profile.

the stellar disk. According to the simulations of Piskunov & Wehlau (1990) this is sufficient because their test inversions with artificial data showed a reasonably correct recovery of the input image even when only five resolution elements were available. Nevertheless, we performed a series of simulations with two rather complicated, artificial input images but otherwise parameters identical to the ones used for mapping EK Draconis. Two of these simulations are shown in Fig. 5.

The two left images in Fig. 5 are the artificial input and the other maps are the recovered images with  $v \sin i = 17.5 \text{ km s}^{-1}$  and  $50 \text{ km s}^{-1}$ , respectively. The simulation in the lower panels may represent a hypothetical spot distribution of an active solar-type star with a band of randomly distributed little cool spots as well as bright plages all over the place plus additional small cool features at and near the pole. The upper simulation in Fig. 5, on the other hand, is a complicated test pattern very tough to reconstruct, even in the most favorable case. All reconstructions were performed with a phase spacing identical to our observations of EK Dra and used the Fe I 6430 line with ten blends. The other input parameters were set to the values as listed in Table 1 and Table 2. Signal-to-noise ratio was adopted to be infinite.

Both reconstructions immediately show the major shortcomings of any Doppler imagery of EK Dra. First, and most notably, are the blurred surface features due to the low spatial resolution of  $13^\circ$  on the stellar surface (determined by the amount of phase smearing and the spectral resolution of  $2.5 \text{ km s}^{-1}$ ). Second, the global redistribution of temperature to conserve the total flux (actually to reproduce the line equivalent width) leads to smaller contrast in the recovered map, i.e. smaller temperature differences between spotted and unspotted photosphere and, third, a general shift of equatorial features to the sub-earth latitude at  $90^\circ - i = 30^\circ$ . One isolated, cool spot at  $\ell \approx 180^\circ$  and a latitude of  $+70^\circ$  erroneously appeared as an “appendage” of the polar feature at about the same latitude in

the  $v \sin i = 17.5$  reconstruction, while it was correctly recovered at higher spatial resolution. Nevertheless, in spite of the expected shortcomings at such a low  $v \sin i$ , the reconstructions clearly preserve the general surface features.

#### 4.4. Doppler imaging of EK Dra

Fig. 6 shows two examples of our observations and their reconstructed profiles – one from each of the two instrumental set-ups. From a series of test runs we find that the optimal reduction of the squared residuals is achieved with a projected, equatorial velocity of  $17.3 \pm 0.4 \text{ km s}^{-1}$ , a radial velocity of  $-23.0 \text{ km s}^{-1}$ , and an inclination of  $\approx 60^\circ$ . All other relevant stellar parameters were obtained by finetuning the reconstructions with these three parameters kept fixed and led to profiles with equivalent widths perfectly compatible with solar abundances when the transition probabilities of Table 2 are used. Modified transition probabilities of the many blends included in the local-line computation were previously listed by Strassmeier (1997) and Weber & Strassmeier (1998). Otherwise they were taken from the line list of Kurucz (1993). We note that the radial velocities from a set of seven moderate-resolution spectra ( $\lambda/\Delta\lambda = 38,000$ ), that we obtained at KPNO in March 1994, are in good agreement with the CFHT velocities one year later and that the short-term constancy of the radial velocity of EK Dra is thus confirmed and well determined. Dorren & Guinan (1994) estimated the inclination of the rotational axis between  $60^\circ$  and  $90^\circ$  from the photometric period, an average  $v \sin i$ , and an assumed stellar radius of  $0.92 R_\odot$  and adopted  $i = 60^\circ$  for their spot modeling. Our test inversions with inclinations between  $20^\circ$  and  $90^\circ$  did indeed result in better fits for  $i > 55^\circ$  but did not reveal a particular significant minimum above that limit. This is basically because the Doppler-imaging technique becomes increasingly insensitive to inclination effects once  $i$  is above  $60^\circ$ ; the nominal value of  $i = 60^\circ$  was adopted.

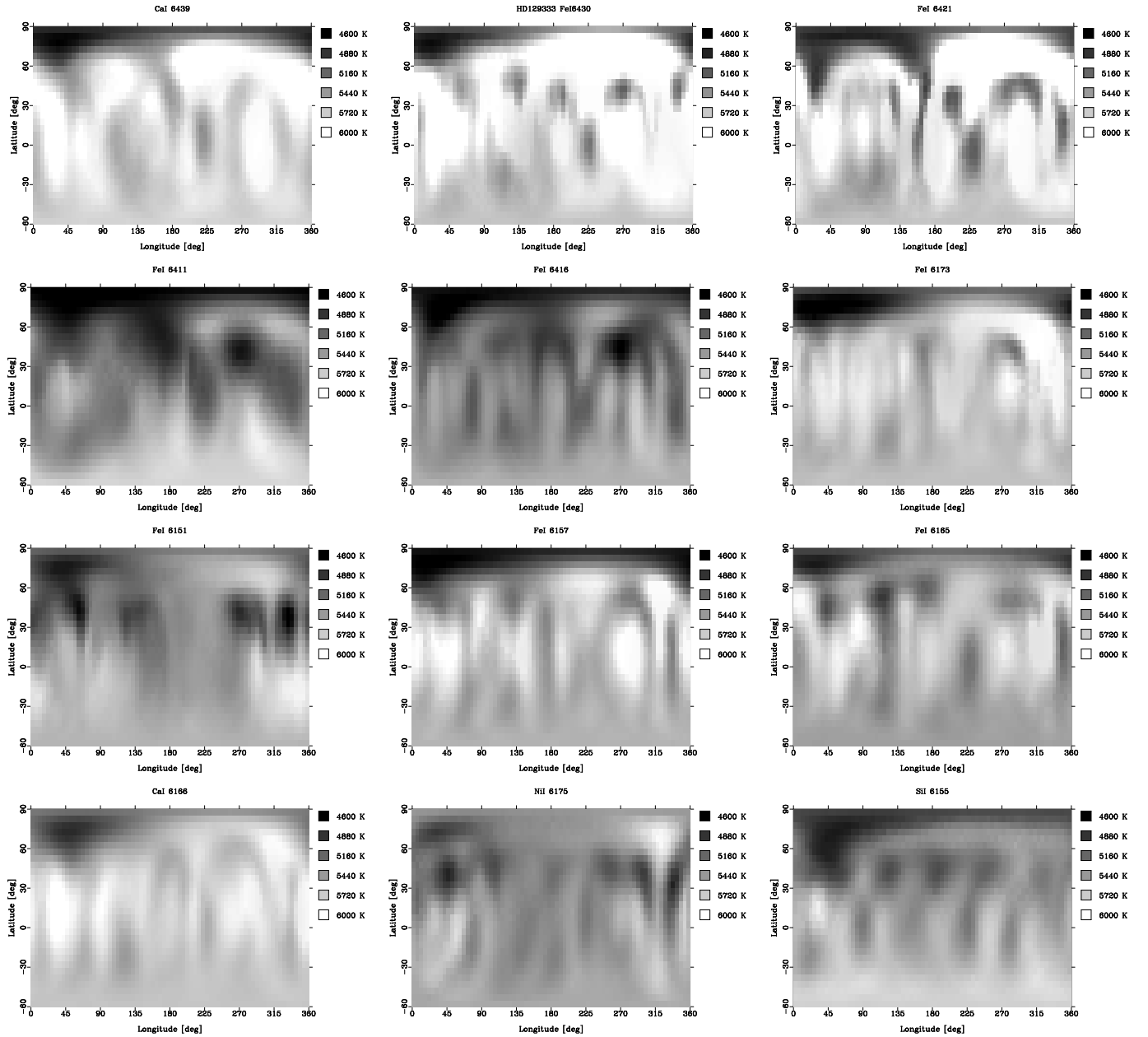


**Fig. 7.** Plots of the reconstructed surface maps for EK Dra from the individual spectral regions. Each map is a pseudo-Mercator projection and plots temperature in Kelvin. The main spectral line is identified at the top of each map and refers to the spectral regions listed in Table 2.

The narrow lines of EK Dra introduced a stronger than usual  $v \sin i$  dependence of the overall temperature contrast of our maps. Equatorial velocities between  $19.0$  and  $20.5 \text{ km s}^{-1}$  were the only ones that led to reasonable maps, i.e. maps without any alternate bright-dark patterns of unrealistic large gradient (either along constant longitudes or latitudes). Increasing or decreasing the equatorial input velocity by yet another  $0.5 \text{ km s}^{-1}$  basically confirms the robustness of our inversion code in that these solutions still reveal a similar spot *pattern* but had either a prohibitively large dark or bright band centered at the sub-stellar latitude and were of significantly larger  $\chi^2$ . We notice

that the stronger lines develop a very cool polar cap of increasing contrast once  $v_{\text{eq}} < 19.5 \text{ km s}^{-1}$ , but that some of these lines – most noticeably CaI 6439 and FeI 6430 – could be fitted without a significant polar cap once  $v_{\text{eq}} > 20.0 \text{ km s}^{-1}$ . Such a strong dependence on the adopted  $v \sin i$  is not seen for the weaker lines. For these lines, the above mentioned full range of  $19.0$ – $20.5 \text{ km s}^{-1}$  results in consistent maps. Consequently, all spectral regions were first inverted with three trial values for  $v_{\text{eq}}$ :  $19.5$ ,  $20.0$ , and  $20.5 \text{ km s}^{-1}$ , corresponding to a  $v \sin i$  of  $16.9$ ,  $17.3$  and  $17.7 \text{ km s}^{-1}$  in order to evaluate the dependence of the results on the choice of this parameter. The finally adopted

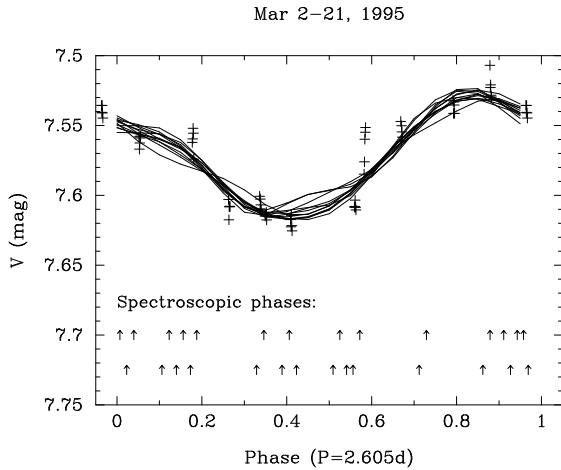


**Fig. 8.** Observed and computed Strömgren- $y$  light curve. The pluses are the observations between March 2–21, 1995 and the lines are the fits from the individual Doppler maps in Fig. 7. Arrows mark the spectroscopic observations in the 6160-Å region (top) and the 6420 Å region (bottom). Note that the  $y$  magnitudes were transformed to Johnson  $V$  for better comparison with Fig. 2.

rotational velocity of  $17.3 \pm 0.4 \text{ km s}^{-1}$  was not only the average of the three trial velocities but also the value that resulted in the most consistent maps from the different line regions and had overall the smallest residuals. These maps are displayed in Fig. 7.

The individual data sets are fitted with a typical sum of the squared residuals of 0.3 which includes the residuals from the single-band photometric fit. The contemporaneous photometric observations of EK Dra and their fits from the line-profile inversions are displayed in Fig. 8.

The total number of iterations was limited to 15 per solution. The first 10 out of the 15 iterations were set to shift full weight to the line profiles and only the remaining five iterations allowed 20% weight for the photometry and 80% for the line profiles.

## 5. Summary and conclusions

The maps from the individual spectral regions are compared in Fig. 7. Fig. 9 shows their latitudinal temperature distributions. The latter graph highlights the preferred latitudes of the spotted regions on EK Draconis in March 1995, i.e.  $+40^\circ$  and  $\approx 70\text{--}90^\circ$ , and were derived by binning all pixels along constant latitudes. Binning width was five degrees starting from the “southern” limb of the stellar disk at a latitude of  $-60^\circ$  up to the visible pole. The thin lines are from the individual maps while the thick line is from the average map. The surface integrated photospheric temperature of EK Dra from all lines was 5520 K in 1995 (shown as a straight dashed line in Fig. 9).

There is abundant (and also consistent) detail in the maps in Fig. 7. Most noticeably is the large high-latitude feature centered at  $\ell \approx 45^\circ$ . It is recovered as part of a polar cap-like spot in 9 out of the 12 maps but seen as an isolated, *very* high-latitude spot without a polar cap in two maps (FeI 6151 and NiI 6175)

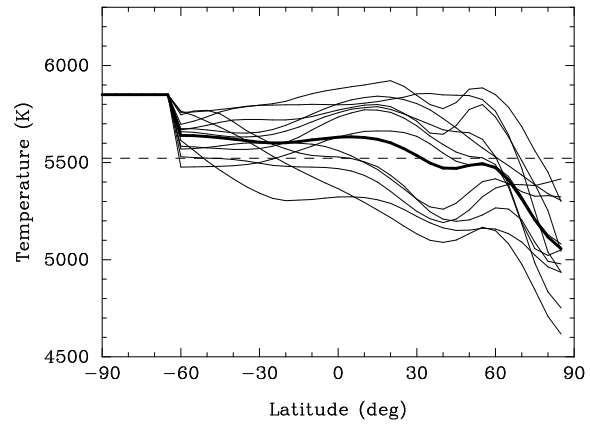


**Fig. 9.** A plot showing the average temperature distribution on EK Dra along constant latitudes. The thin lines are from the individual maps and the thick line is from the average map. The dashed line represents the grand average surface temperature from all lines. The value below a latitude inclination of  $-60^\circ$  is the adopted, effective photospheric temperature of 5850 K from Table 1.

while yet another map (CaI 6166) may be an intermediate case. The two lines clearly without a polar cap are weak lines of similar equivalent width but different temperature sensitivity ( $\chi_{\text{low}} = 2.2$  vs. 4.1 eV) but, since the other lines with a polar cap span an even larger range of equivalent width (a factor of over 6) and excitation potential (2.1–5.6 eV), they do not stand out by means of their atomic parameters. Other weak lines also lead to a significant polar feature, e.g. from FeI 6157 or FeI 6416, but the strong lines always do. However, in any case the polar feature on EK Dra is smaller – but not relatively warmer – than on more rapidly rotating RS CVn-type binaries or the ultra-fast rotating single ZAMS stars. The spot morphology on EK Dra would fit into the *ad hoc* hypothesis of lesser polar-field emergence, i.e. polar spots, the slower a star rotates or, for dwarf stars of approximately identical internal structure, the further it is away from the ZAMS. Because of the relatively low  $v \sin i$  of EK Dra and its resulting uncertainties, we consider the existence of a small polar cap on EK Dra as inconclusive until verified. On the other hand, the *very* high-latitude feature at  $b > 60^\circ$  and at  $\ell \approx 45^\circ$  is well constrained by all our maps and could be termed a “polar” spot as well.

Further detail includes an equatorial spot at  $\ell \approx 225^\circ$  and three medium-latitude ( $b \approx 30\text{--}50^\circ$ ) spots at longitudes of  $45^\circ$  (the extension of the polar feature),  $180^\circ$ , and  $270^\circ$ , respectively. The latitude of a fourth feature at  $\ell \approx 130^\circ$  can not be uniquely determined because it appears mirrored by a similarly large spot in the opposite hemisphere at  $b \approx -20^\circ$  and is thus suspicious. A fifth feature is recovered at around  $\ell \approx 330^\circ$ . Its shape and overall appearance, however, is rather diverse but in several maps consistently reconstructed; as a double, elongated, cool spot with a sharp separation from FeI 6157, NiI 6175, FeI 6421, FeI 6416 (and possibly also from FeI 6430, FeI 6151, and CaI 6166, the latter with significantly less contrast though), as a single blurred feature from FeI 6411, SiI 6155 and CaI 6439,

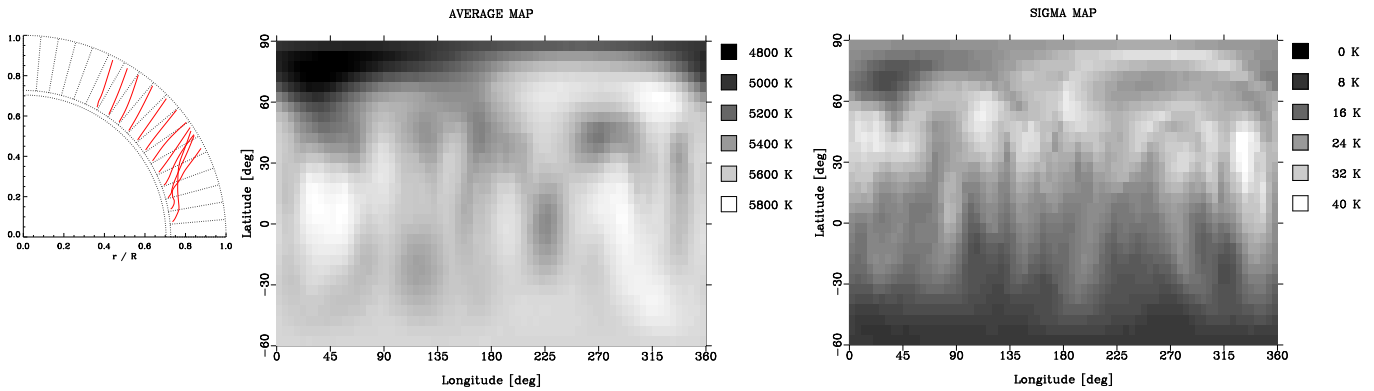


**Fig. 10.** A comparison of the average Doppler image of EK Dra in pseudo-Mercator projection (middle panel; left of the two maps) and a stellar model showing the meridional projection of trajectories of rising flux tubes through the convection zone and the predicted latitude distribution of their emerging magnetic fields (very left graph). The “map” to the right shows the standard deviations from the mean in units of temperature per surface pixel (note, the darker the better the agreement).

or is simply absent as in the map from FeI 6173. There seems to be no tendency with atomic line parameters like excitation potential, i.e. temperature sensitivity, or line strength.

Finally, the left map in Fig. 10 shows the unweighted average Doppler image of EK Dra and intends to highlight the *consistent* details from the individual-line maps while the other map in Fig. 10 plots the standard deviations of the mean per surface pixel. Visual comparison of these two maps allows to judge the reliability of particular surface features. We see that the “polar” spot at  $b \approx 60 - 80^\circ$  and  $\ell \approx 45^\circ$  is the most consistent feature of all while the weak spot at  $\ell \approx 330^\circ$  is the least reliable of the spots that survived the averaging.

For comparison purposes, we used an updated version of the MHD code of Schüssler et al. (1996) to generate trajectories of the rising, toroidal, flux tubes for a stellar model matching EK Draconis (for details see Granzer et al. 1997). The stellar crosssection in the left panel in Fig. 10 with the tube’s predicted emerging latitudes can be directly compared to our average Doppler image. But while the model predicts spots only between latitudes of  $25-65^\circ$ , with a preferred emergence at  $30-35^\circ$ , our Doppler image shows also spots at significantly higher and lower latitudes. Part of the discrepancy may very well be, e.g., with the poleward slip of loops already formed at very high latitudes (e.g. DeLuca et al. 1993) but not taken into account in the models. Or, the dynamo might be of qualitatively different design than the solar boundary-layer dynamo as could be suspected by the rapid rotation of EK Dra when compared to the Sun. EK Dra’s Rossby number ( $\equiv P_{\text{rot}}/\tau_{\text{conv}}$ ) is 0.12 (with  $\tau_{\text{conv}} \approx 22$  days), thus well below the solar value of 1.0 and the 0.65 threshold for the onset of heavy spottedness as found by Hall (1994).

The existence of polar cap-like spots has been criticized in the literature on the basis that Doppler imaging mainly relies on the correctly adopted local line profile, or in other words, on the reference “zero point” of the spectral line deformations (Byrne 1996). One important line of Byrne’s arguments is that active stars are highly magnetic and their atmospheric structure gradi-

ents may differ significantly from inactive reference stars as well as plane parallel, LTE model atmospheres. Although a possible scenario, two recent publications found convincing evidence that this can not remove polar spots. First, non-LTE computations of the usual Doppler-imaging lines for spun-up solar-type stars reveal no significant signatures from plage regions (Bruls et al. 1997; see also Stout-Batalha & Batalha 1996) and, second, Doppler images of AB Doradus from the very strong and completely saturated NaI-D lines show basically the same feature as the much weaker lines (Unruh & Cameron 1997), thereby excluding chromospheric-activity effects in the line core as the cause of the polar spot of AB Doradus.

In this paper we presented yet another star with a very high-latitude, or even polar spot, whose presence is unambiguous within the framework of our analysis and repeatedly needed by the various line-profile data and input model atmospheres. However, the present result is special because, for the first time, we model a true solar-type star of spectral type G1-2V where most uncertainties and shortcomings of standard model atmospheres are minimized due to many (successful) comparisons of the models with the observed solar spectrum; and a polar spot – or at least a *very* high-latitude spot – is still seen! Of course, EK Dra is rotating ten times more rapidly than the Sun and is located close to the ZAMS, thus its atmospheric structure may still not be directly comparable to the present Sun’s, but it is certainly a much better approximation than an atmosphere of the many K-giant components in RS CVn-type binaries that were first seen with prominent polar spots.

The main conclusion from our temperature images of a young solar twin is that its spot distribution is qualitatively different than the present Sun’s. The existence of a very high-latitude spot, and possibly even a polar cap-like feature, is only qualitatively in agreement with the flux-tube transportation model of Schüssler et al. (1996) and thus requires the addition of a physical process that moves toroidal flux tubes to very high latitudes. Also, we have proven that Doppler imaging can be extended down to stars with  $v \sin i$  as low as  $17.3 \text{ km s}^{-1}$ .

*Acknowledgements.* It is a great pleasure to thank John Glaspey and David Bohlender for their help with *Gecko* and Manuel Güdel for various discussions concerning EK Draconis. JBR acknowledges support from the Natural Science and Engineering Research Council of Canada (NSERC) and KGS is very grateful to the Austrian Fond zur Förderung der wissenschaftlichen Forschung (FWF) for support under grant S7302-AST and S7301-AST.

## References

- Breger M., 1990, Comm. in Asteroseism. 20, 1
- Bruls J. H. M. J., Solanki S. K., Schüssler M., 1997, in Donahue R. & Bookbinder J. (eds.), Proc. 10<sup>th</sup> Cambridge Workshop on Cool Stars, Stellar Systems, and the Sun, PASPC, in press
- Byrne B., 1996, in Strassmeier K. G. & Linsky J. L. (eds.), *Stellar Surface Structure*, IAU Symp. 176, Kluwer, Dordrecht, p. 299
- Canuto V. M., Mazzitelli I., 1992, ApJ 389, 724
- Castelli F., Gratton R. G., Kurucz R. L., 1997, A&A 318, 841
- Chugainov P. F., Lovkaya M. N., Zajtseva G. V., 1991, IBVS 3680
- Collier-Cameron A., 1995, MNRAS 275, 534
- Collier-Cameron A., Unruh Y. C., 1994, MNRAS 269, 814
- DeLuca E. E., Fisher G. H., Patten B. M., 1993, ApJ 411, 383
- Deutsch A., 1958, in Lehnert B. (ed.), *Electromagnetic Phenomena in Cosmological Physics*, IAU Symp. 6, Cambridge Univ. Press, Cambridge, p. 209
- Donati J.-F., Collier-Cameron A., 1997, MNRAS, in press
- Dorren J. D., Guinan E. F., 1994, ApJ 428, 805
- Dorren J. D., Güdel M., Guinan E. F., 1995, ApJ 448, 431
- Granzer T., Strassmeier K. G., Schüssler M., Caligari P., 1997, in Donahue R. & Bookbinder J. (eds.), Proc. 10<sup>th</sup> Cambridge Workshop on Cool Stars, Stellar Systems, and the Sun, PASPC, in press
- Güdel M., Guinan E. F., Mewe R., Kaastra J. S., Skinner S. L., 1997a, ApJ 479, 416
- Güdel M., Guinan E. F., Skinner S. L., 1997b, ApJ, in press
- Güdel M., Schmitt J. H. M. M., Benz A. O., Elias N. M. II, 1995b, A&A 301, 201
- Güdel M., Schmitt J. H. M. M., Benz A. O., 1995a, A&A 302, 775
- Hall D. S., 1994, in D'Antona F. et al. (eds.), *Evolutionary links in the zoo of interactive binaries*, Mem.S.A.It. 65, p. 73
- Hatzes A. P., 1995, in Strassmeier K. G. (ed.), *Poster Proceedings: Stellar Surface Structure*, IAU Symp. 176, Univ. of Vienna, p. 90
- Henry G. W., Eaton J. A., Hamer J., Hall D. S., 1995, ApJS 97, 513
- Hussain G. A. J., Unruh Y. C., Collier Cameron A., 1997, MNRAS, in press
- Kupka F., 1996, in Strassmeier K. G. & Linsky J. L. (eds.), *Stellar Surface Structure*, IAU Symp. 176, Kluwer, Dordrecht, p. 557
- Kürster M., Schmitt J. H. M. M., Cutispoto G., 1994, A&A 289, 899
- Kurucz, R. L., 1993, ATLAS-9, CD-ROM No. 13
- Piskunov N. E., 1996, in Strassmeier K. G. & Linsky J. L. (eds.), *Stellar Surface Structure*, IAU Symp. 176, Kluwer, Dordrecht, p. 45
- Piskunov N. E., Rice J. B., 1993, PASP 105, 1415
- Piskunov N. E., Wehlau W. H., 1990, A&A 233, 497
- Radick R. R., 1991, in C. P. Sonett et al. (eds.), *The Sun in Time*, Univ. of Arizona Press, p. 787
- Ramseyer T. F., Hatzes A. P., Jablonski F., 1995, AJ 110, 1364
- Rice J. B., Strassmeier K. G., 1997, A&A, in prep. (paper VII)
- Rice J. B., Wehlau W. H., Khokhlova V. L., 1989, A&A 208, 179
- Saar S. H., Bookbinder J., 1997, in Donahue R. & Bookbinder J. (eds.), Proc. 10<sup>th</sup> Cambridge Workshop on Cool Stars, Stellar Systems, and the Sun, PASPC, in press
- Saar S. H., Piskunov N. E., Tuominen I., 1994, in Caillault J.P. (ed.), Proc. 8<sup>th</sup> Cambridge Workshop on Cool Stars, Stellar Systems, and the Sun, PASPC 64, p. 661
- Scheible M. P., Guinan E. F., 1994, IBVS 4110
- Schüssler M., Caligari P., Ferriz-Mas A., Solanki S. K., Stix M., 1996, A&A 314, 503
- Smalley B., Kupka F., 1997, A&A, in press
- Soderblom D. R., 1985, AJ 90, 2103
- Stout-Batalha N. M., Vogt S. S., 1996, in Strassmeier K. G. & Linsky J. L. (eds.), *Stellar Surface Structure*, IAU Symp. 176, Kluwer, Dordrecht, p. 337
- Stout-Batalha N. M., Batalha C. C., 1996, in Pallavicini R. & A. K. Dupree (eds.), Proc. 9<sup>th</sup> Cambridge Workshop on Cool Stars, Stellar Systems, and the Sun, PASPC 109, p. 631
- Strassmeier K. G., 1997, A&A 319, 535 (paper III)
- Strassmeier K. G., Bartus J., Cutispoto G., Rodonó M., 1997a, A&AS 125, 11
- Strassmeier K. G., Bopp B. W., 1992, A&A 259, 183
- Strassmeier K. G., Boyd L. J., Epan D. H., Granzer T., 1997b, PASP 109, 697
- Strassmeier K. G., Rice J. B., Wehlau W. H., Hill G. M., Matthews J., 1993, A&A 268, 671
- Unruh Y. C., Collier-Cameron A., 1997, MNRAS, in press
- Unruh Y. C., Collier-Cameron A., Cutispoto G., 1995, MNRAS 277, 1145
- Vogt S. S., Penrod G. D., 1983, PASP 95, 565
- Vogt S. S., Penrod G. D., Hatzes A. P., 1987, ApJ 321, 496
- Weber M., Strassmeier K. G., 1998, A&A, in press (paper V)